Covalent Organic Framework Thin-film Photodetectors from Solution Processable Porous Nanospheres

Bag, S.; Sekhar Sasmal, H.; Pratap Chaudhary, S.; Dey, K.; Blätte, D.; Guntermann, R.; Zhang, Y.; Položij, M.; Kuc, A. B.; Shelke, A.; Vijayaraghavan, R. K.; Ajithkumar, T. G.; Bhattacharyya, S.; Heine, T.; Bein, T.; Banerjee, R.;

Originally published:

January 2023

Journal of the American Chemical Society 45(2023)3, 1649-1659

DOI: https://doi.org/10.1021/jacs.2c09838

Covalent Organic Framework Thin-film Photodetectors from Solution Processable Porous Nanospheres

Journal:	*Journal of the American Chemical Society*
Manuscript ID	ja-2022-09838w
Manuscript Type:	Article
Date Submitted by the Author:	15-Sep-2022
Complete List of Authors:	Bag, Saikat; Indian Institute of Science Education and Research Kolkata, Department of Chemical Sciences Sasmal, Himadri; National Chemical Laboratory CSIR, Chaudhary, Sonu; Indian Institute of Science Education and Research Kolkata, Chemistry DEY, KAUSHIK; IISER Kolkata Department of Chemical Sciences, Chemical Sciences Blaette, Dominic; Ludwig-Maximilians-Universität München, Department of Chemistry and Center for NanoScience (CeNS), Guntermann, Roman; Ludwig-Maximilians-Universität München Zhang, Yingying; TU Dresden, Faculty of Chemistry and Food Chemistry, Položij, Miroslav; Technische Universität Dresden, Faculty of Chemistry and Food Chemistry Kuc, Agnieszka; Helmholtz-Zentrum Dresden-Rossendorf, Shelke, Ankita; National Chemical Laboratory CSIR, Central NMR Facility and Physical/Materials Chemistry Division Vijayaraghavan, Ratheesh; Indian Institute of Science Education and Research Kolkata, Department of chemical Sciences Ajithkumar, Thalasseril; National Chemical Laboratory CSIR, Central NMR Facility Bhattacharyya, Sayan; Indian Institute of Science Education and Research Kolkata, Chemistry Heine, Thomas; TU Dresden, School of Science Bein, Thomas; Ludwig-Maximilians-Universität München Banerjee, Rahul; Indian Institute of Science Education and Research Kolkata, Department of Chemical Sciences; Indian Institute of Science Education and Research Kolkata, Department of Chemical Sciences

Covalent Organic Framework Thin-film Photodetectors from Solution Processable Porous Nanospheres

Saikat Bag,[1,2†] Himadri Sekhar Sasmal,[1,2†] Sonu Pratap Chaudhary,[1,2†] Kaushik Dey,[1,2] Dominic Blätte,[3] Roman Guntermann,[3] Yingying Zhang,[4] Miroslav Položij,[4] Agnieszka Kuc,[5] Ankita Shelke,[6] Ratheesh K Vijayaraghavan[1,2] Thalasseril G. Ajithkumar,[6] Sayan Bhattacharyya,[1,2*] Thomas Heine,[4,5,7*], Thomas Bein[3*] and Rahul Banerjee[1,2*]

[1]Department of Chemical Sciences, Indian Institute of Science Education and Research, Kolkata, Mohanpur 741246, India.

[2]Centre for Advanced Functional Materials, Indian Institute of Science Education and Research, Kolkata, Mohanpur 741246, India.

[3]Department of Chemistry and Center for NanoScience (CeNS), Ludwig-Maximilians- Universität München, Butenandtstrasse 5-13 (E), 81377 Munich, Germany.

[4]Faculty of Chemistry and Food Chemistry, TU Dresden, Bergstrasse 66c, 01069 Dresden, Germany.

[5]Helmholtz-Zentrum Dresden-Rossendorf, Abteilung Ressourcenökologie, Forschungsstelle Leipzig, 04318 Leipzig, Germany.

[6]Central NMR Facility and Physical/Materials Chemistry Division, CSIR-National Chemical Laboratory, Dr. Homi Bhabha Road, Pune 411008, India.

[7]Department of Chemistry, Yonsei University and ibs center for nanomedicine, 50 Yonsei-ro, Seodaemun-gu, Seoul 03722, Republic of Korea.

*Email: sayanb@iiserkol.ac.in; Tel: +033-6136-0000-1275.

*Email: bein@lmu.de; Tel: +49-89 2180 77621.

*Email: thomas.heine@tu-dresden.de; Tel: +49 351 463 37637.

*Email: r.banerjee@iiserkol.ac.in; Tel: +033-6136-0000-1327.

ABSTRACT: The synthesis of homogeneous covalent organic framework (COF) thin films on the desired substrate with decent crystallinity, porosity, and uniform thickness has great potential for optoelectronic applications. We have used a solution-processable sphere transmutation process to synthesize 300±20 nm uniform COF thin films on a 2×2 cm^2 TiO_2-coated FTO surface. This process controls the nucleation of COF crystallites and molecular morphology that helps the nanospheres to arrange periodically to form homogeneous COF thin films. We have synthesized four COF thin films (TpDPP, TpEtBt, TpTab, and TpTta) with different functional backbones. In a close agreement between the experiment and density functional theory, the TpEtBr COF film showed the lowest optical bandgap (2.26 eV) and highest excited-state lifetime (8.52 ns) among all four COF films. Hence, the TpEtBr COF film can participate in efficient charge generation and separation. We constructed optoelectronic devices having a glass/FTO/TiO_2/COF-film/Au architecture, which serves as a model system to study the optoelectronic charge transport properties of COF thin films under dark and illuminated conditions. The visible light with a calibrated intensity of 100 mW cm^{-2} was used for the excitation of COF thin films. All the COF thin films exhibit significant photocurrent after illumination with visible light in comparison to the dark. Hence, all the COF films behave as good photoactive substrates with minimal pin hole defects. The fabricated out-of-plane photodetector device based on the TpEtBr COF thin film exhibits high photocurrent density (2.65 ± 0.24 mA cm^{-2} at 0.5 V) and hole mobility (8.15±0.64 ×10^{-3} cm^2 V^{-1} S^{-1}) compared to other as-synthesized films, indicating the best photoactive characteristics.

INTRODUCTION

Two-dimensional (2D) covalent organic frameworks (COFs) are lightweight materials that consist of organic molecular subunits.[1,2] Long-range order, high surface area, as well as a vast range of possible molecular building blocks make these materials intriguing candidates for energy harvesting[3,4] and storage. Consequently, COFs with a photoactive functional backbone can exhibit promising optoelectronic properties[5] for applications[6-10] like

photosensitization, light-harvesting, in logic gates, and for memory devices. Gaining control over the orientation of COF layers relative to a substrate is a prerequisite for investigating the in-plane/out-of-plane charge migration[11,12]. Several protocols such as residual crystallization, interfacial polymerization and solvothermal synthesis have been reported for COF thin film construction on substrates.[13,14] However, often these methods are limited to selected COFs or the morphology of the resulting COF thin films is still unsatisfactory for uniform and planar device fabrication, which is essential for precisely characterizing charge transport properties[15-17]. In addition, controlling the morphology and microstructure during the COF thin film formation would be possible avenues to obtain improved charge transport.

Herein, we report a solution-processable sphere transmutation process where the first step involves the nucleation and growth of reactive COF nanospheres in solution. In the second step, the COF nanospheres have been recrystallized on the TiO_2-coated FTO surface. In the process of such recrystallization, they were transmuted into crystalline, porous, crack-free COF thin films with a uniform thickness of ~300 nm. The COF thin film maintains the band energy alignment, structural geometry, and π-column density that control the generation and separation of photogenerated excitons and the charge carrier lifetime, as also shown in our density functional theory (DFT) simulations. Such a control tunes the photophysical properties[18,19] like current density, charge-carrier mobility, charge-transfer resistance, capacitance, and dielectric constant, which are all in close agreement with the results of DFT calculations for crystalline bulk systems. Here, we used the sphere transmutation strategy to synthesize four COF thin films (TpDPP, TpEtBr, TpTab, and TpTta) with different functional backbones. The rationale behind using four different linkers is to understand electronic communication and charge carrier delocalization to assess their effects on optical properties and charge transport. The four COF thin films behave as photoactive materials and show moderate to high current-density and charge-carrier mobility under light illumination.

RESULTS AND DISCUSSION

Although COF thin films have been reported as photoabsorbers, the photovoltaic performance achieved so far is still limited.[4-11] The synthetic strategy to obtain oriented COF thin films with minimum surface roughness is still not generic. Therefore, we developed a solution-processable sphere transmutation approach for synthesizing COF thin films. In this process, the reaction occurs in very dilute conditions, preventing the precipitation of an amorphous phase and slowing down the crystallization process to generate crystalline COF nanospheres. Briefly, to synthesize TpDPP and TpEtBr, 0.045 mmol of diamine linkers [3,8-diamino-6-phenylphenanthridine (DPP, 12.8 mg); 5-ethyl-6-phenyl-phenanthridine-3,8-diamine bromide (EtBr, 17.7 mg)] were dissolved in 100 mL dry dichloromethane (DCM). Similarly, for TpTab and TpTta, 0.03 mmol of triamine linkers [1,3,5-tris(4-aminophenyl) benzene (Tab, 10.6 mg); 4,4',4''-(1,3,5-triazine-2,4,6-triyl) trianiline (Tta, 10.7 mg)] were dissolved in a 50 mL dry acetonitrile (ACN) and 50 mL dry DCM. The amine solutions were kept at 30 °C in a closed system for 10 minutes. Trifluoroacetic acid (TFA) was added to the amine solution as the catalyst. Then, 0.03 mmol of trialdehyde [1,3,5–triformylphloroglucinol (Tp, 6.3 mg)] in 100 mL DCM was added to the acidic solution of amine and 2×2 cm^2 sized anatase-smoothed TiO_2-coated FTO was gently placed in the reaction. The reaction mixture was refluxed at 60-70 °C and kept for 24 h (Figure S1). The nanospheres self-assemble in the solid-liquid interface and start recrystallizing to form an oriented COF thin film with high crystallinity and porosity (Figure 1a-b, S2). The crystallite growth was completed parallel to the substrate and well-adhered TpDPP, TpEtBr, TpTab, and TpTta COF thin films were grown on the TiO_2-coated FTO surface after 24 h (Figure S3). Powder X-ray diffraction (PXRD) was utilized to verify the ordered structures of as-synthesized COF thin films. The peak at 3.6 ± 0.2°(2θ) for TpDPP, 3.8 ± 0.2° (2θ) for TpEtBr, 5.7 ± 0.2° (2θ) for TpTab, and 5.8 ± 0.2° (2θ) for TpTta indicate the crystallization along the (100) planes. The diffraction from the (100) planes of TpTab and TpTta exhibit peaks at higher 2θ values, because of their smaller pore apertures and unit cell dimensions. The peaks at ~26°-27° manifested from the (001) plane reflection demonstrate the π-π interaction between the COF layers (Figure 1c-f). We have constructed theoretical model structures of these thin films using the SCC-DFTB method[20] with the 3ob-3-1 parameter set[21] in the AMS program suite[22]. To simulate their PXRD patterns, we used statistical models developed in previous work[23] with 50 COF layers of different stackings (see details in the Supporting Information SI-10 and Figures S14, S17, and S19). These models generate simulated PXRD patterns that are in close agreement with their experimental counterparts. Then, to facilitate calculations at a higher level of theory, we cut out smaller statistical models with four layers for TpDPP and TpEtBr and six layers for TpTab and TpTta, to simulate their electronic properties. TpDPP COF layers are constructed by the mixture of the framework's slipped AA-direct (denoted AA'-direct) with syn and anti-orientation. Random anti-orientation of the AA'-direct model structure is preferred for the TpEtBr thin film layers. The mixture of AA and AA'-direct and AA-rotated backbone is favorable for TpTta and TpTab (Figure 3a-d, S13, S15, S16, and S18). Experimental PXRD patterns matched well with the simulated patterns of (a) the mixture of AA'-direct-syn and AA'-direct-anti for TpDPP, (b) AA'-direct-anti for TpEtBr, (c) the mixture of AA/AA'-direct and AA/AA'-rotated for TpTab and TpTta stacking models (Figure 3a-d). We performed the Pawley refinement, which showed good agreement [TpDPP (R_P = 3.67%, R_{WP} = 1.77%); TpEtBr (R_P = 4.01%, R_{WP} = 1.85%); TpTab (R_P = 1.36%, R_{WP} = 0.65%); TpTta (R_P = 0.47%, R_{WP} = 0.23%)] between the simulated and the experimental diffraction patterns (Figure S6).

The FT-IR spectra showed characteristic stretching bands of the as-synthesized COF films at 1621-1623 cm^{-1} (–C=O), 1573-1576 cm^{-1} (–C=C), and 1248-1291 cm^{-1} (-C–N) indicating the formation of a β-ketoenamine framework backbone (Figure S4). Time-dependent scanning electron microscopy (SEM) and transmission electron microscopy

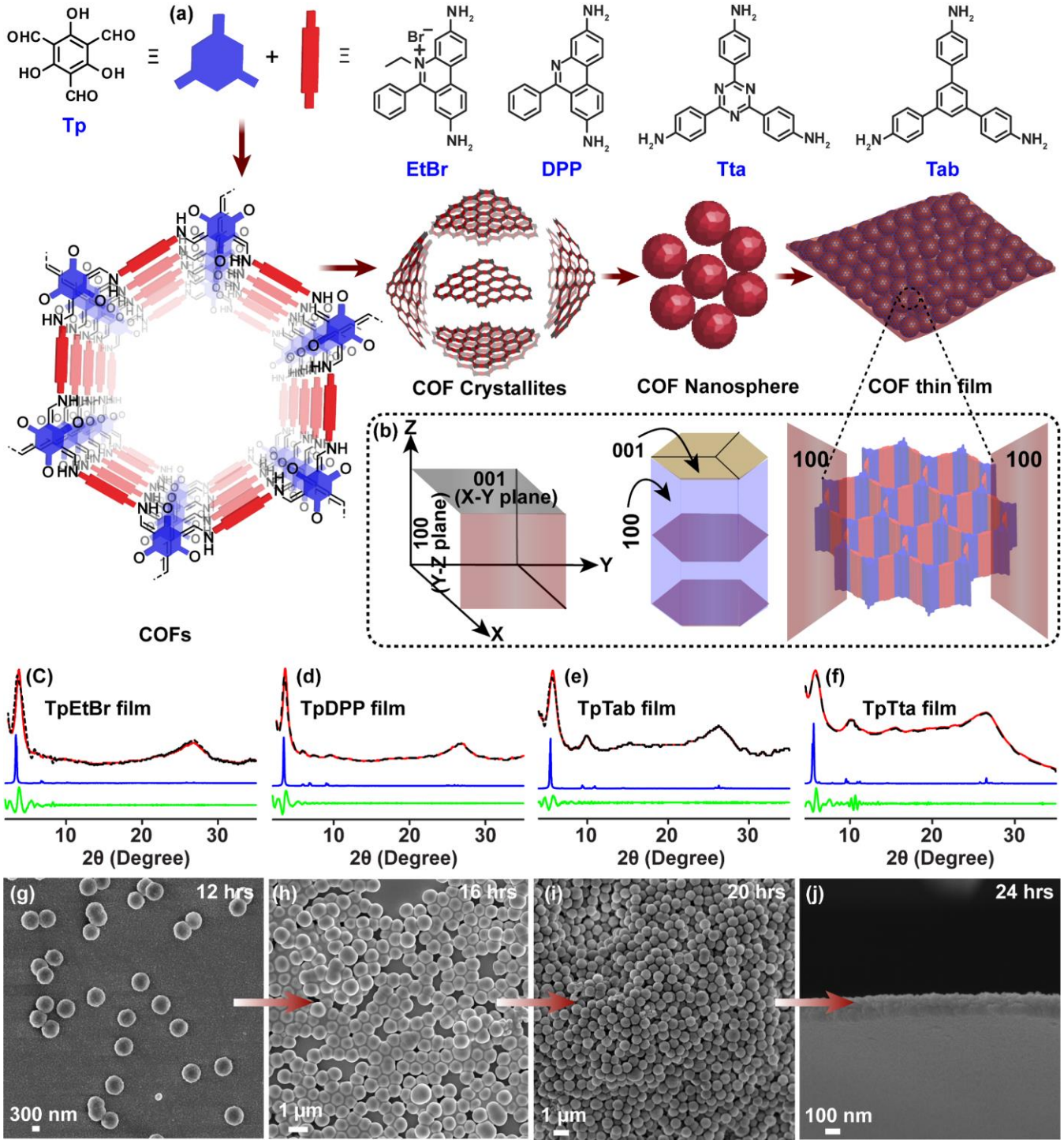

Figure 1. (a) Schematic representation of COF thin film fabrication at TiO_2-coated FTO surface *via* sphere transmutation process. (b) Representation of orientation of (100) plane in the as-synthesized COF thin films. (c-f) Comparison of PXRD patterns between the experimental (red), refined (black), simulated (blue), and Pawley refinement difference (green) of four COF thin films. (g-j) Time-dependent SEM images during the formation of TpDPP COF thin film synthesized by sphere transmutation.

(TEM) of the nanospheres indicate that diamines (DPP, EtBr, Tab, and Tta) react with the trialdehyde (Tp) in the presence of a catalytic amount of TFA within 12 h to form porous and crystalline COF nanospheres with a size range ~700-800 nm (Figure 1, Section S9). These COF nanospheres have free $-NH_2$ (3396 and 3355 cm^{-1}) and –CHO (1718 cm^{-1}) functionalities, which were confirmed by IR spectral analysis (Figure S5). These reactive chemical functionalities influence the subsequent covalent self-assembly of the nanospheres via reversible covalent bond formation. After 16 h, COF nanospheres start to recrystallize in an oriented way on the TiO_2-coated FTO surface. The porous, crystalline, continuous COF thin-film was formed after 24 h with the disappearance of the nanospheres (Figure 1g-j, S10, S11, S12). Time-dependent PXRD analyses were utilized to understand the crystallite

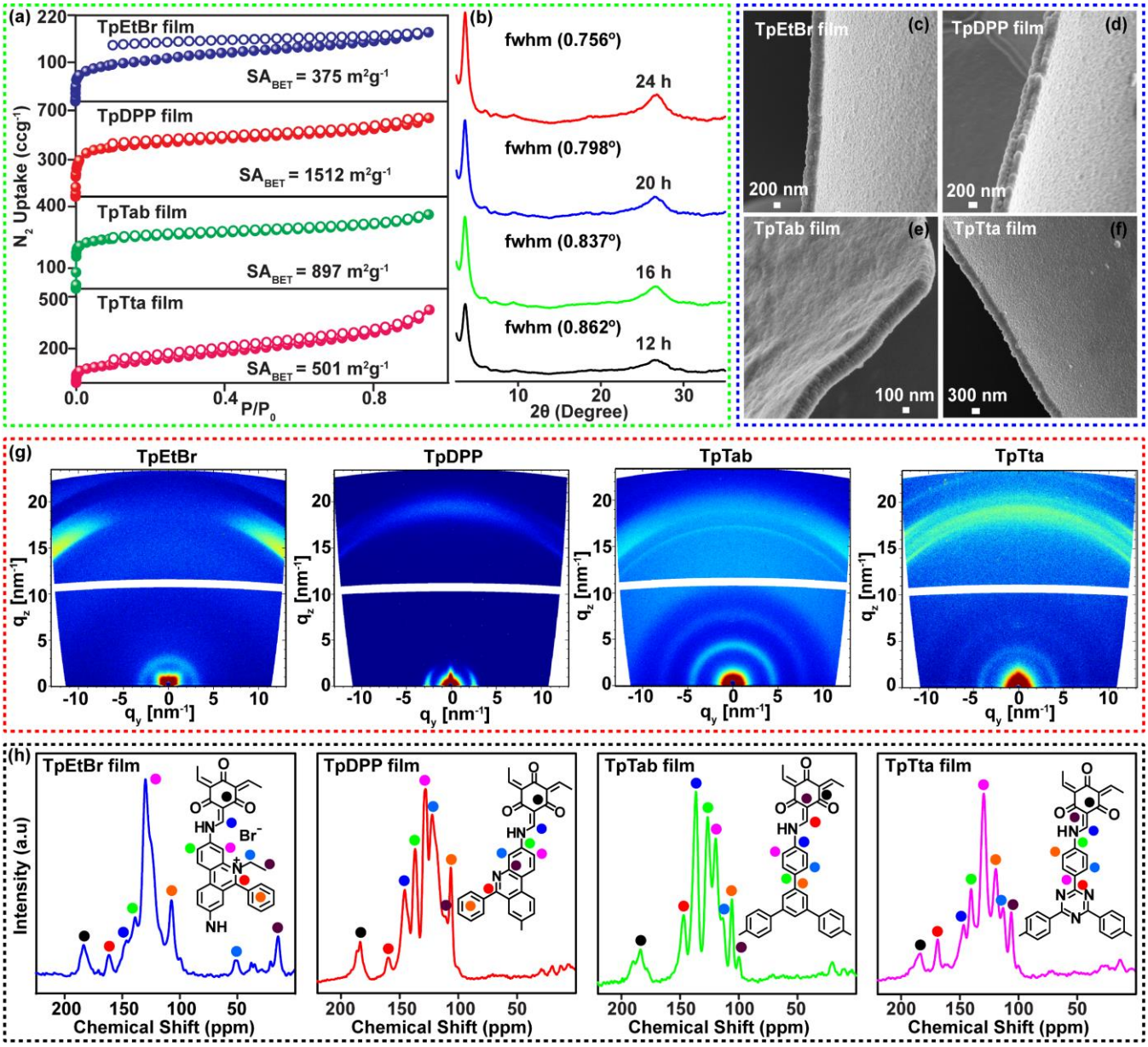

Figure 2. (a) N_2 adsorption isotherms of as-synthesized COF thin films. (b) Time-dependent PXRD patterns of TpDPP COF thin film during the process of sphere transmutation. (c, d, e, and f) SEM images of the TpEtBr, TpDPP, TpTab, and TpTta COF thin films show the crack-free surface. (g) GIXRD patterns of all four COF films. (h) Solid-state ^{13}C CP-MAS NMR spectra of TpEtBr, TpDPP, TpTab, and TpTta COF thin films, respectively.

growth during the thin film formation. We calculated the full width at half-maximum (fwhm) [TpDPP (3.7°)] of the high-intensity peak. The fwhm value of as-synthesized TpDPP COF nanospheres after 12 h of reaction is 0.862°. The nanospheres arranged themselves periodically to minimize the defects, and the fwhm value decreased to 0.837° after 16 h. TpDPP nanospheres were completely transmuted to highly crystalline COF thin films, and the fwhm value was further decreased to 0.756° (Figure 2b). The Brunauer-Emmett-Teller (BET) surface areas of the four thin films are 1512 (TpDPP), 375 (TpEtBr), 897 (TpTab), and 501 (TpTta) m^2g^{-1} with approximate pore diameters of 1.8, 1.9, 1.6, and 1.4 nm, respectively (Figure 2a and S8). Thermogravimetric (TGA) analysis profiles showed that all these thin films are thermally stable up to 400 °C (Figure S9). We performed a grazing-incidence wide-angle X-ray scattering analysis (GIWAXS) of the COF thin films to understand the preferential orientation of layers with respect to the TiO_2-coated FTO surface. GISAXS confirmed that TpDPP COF thin film layers are orientated along the (100) axis, parallel to the substrate's surface (Figure 2g). GIWAXS of TpEtBr, TpTab, and TpTta COF thin films showed good crystallinity but no preferential orientation. This indicates that the TpDPP nanosphere recrystallized on the substrate to form orientated film along the (100) axis. In contrast, such preferential recrystallization was not observed in the case of TpEtBr, TpTab, and TpTta COF thin films. Further time-dependent GIWAXS measurements for TpDPP films confirmed the proposed transmutation process (Figure S7). Only from 14 h and onwards, crystalline and oriented films were observed with comparable quality. Hence, for TpDPP, we propose that the transmutational recrystallization from

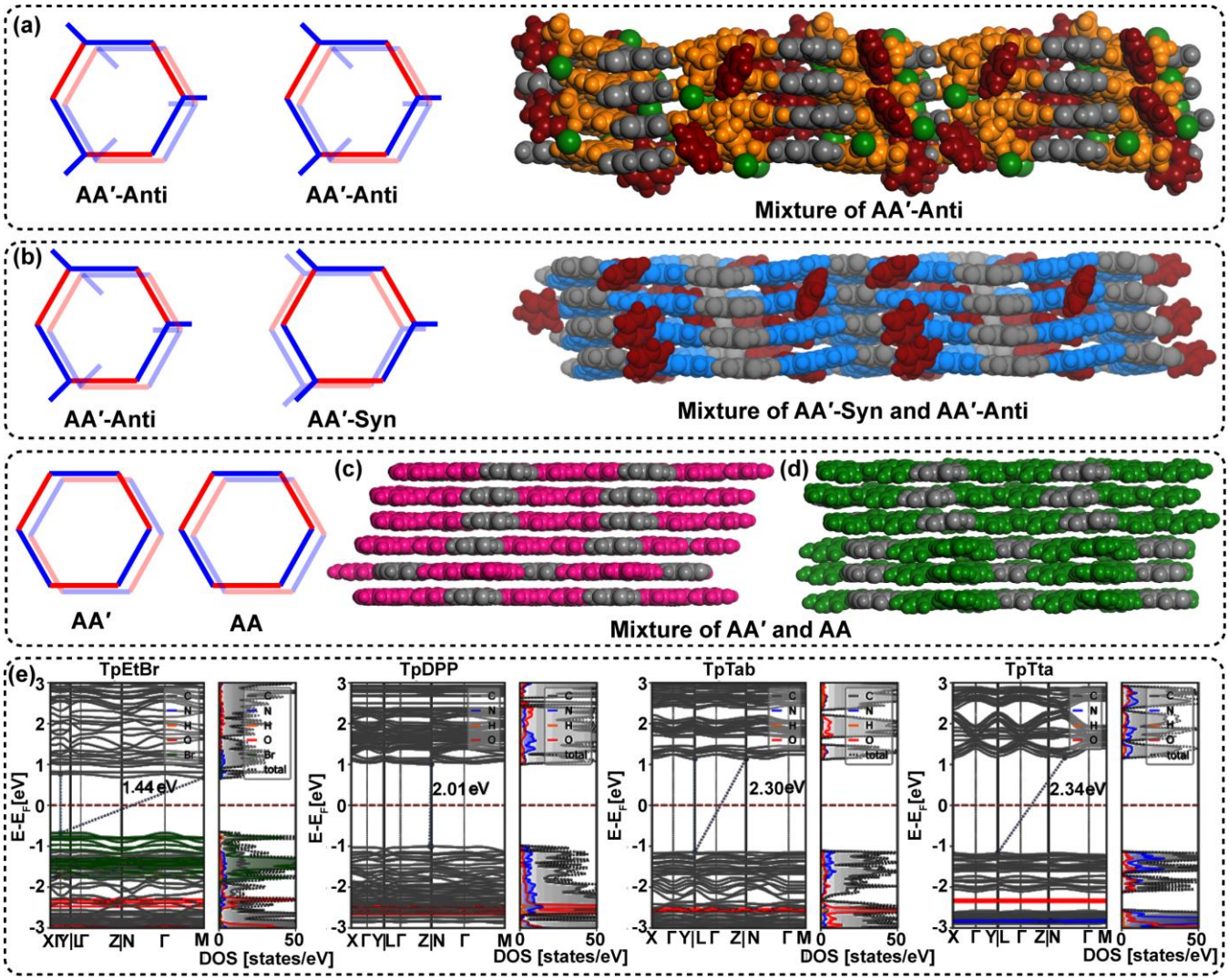

Figure 3. Theoretically constructed and geometry optimized model structures of (a) TpEtBr, (b) TpDPP, (c)TpTta, (d) TpTab COF thin films based on their experimental PXRD patterns. (e) Computationally predicted electronic band structure of four COF thin films.

nanospheres to film occurs faster or at least at a similar time scale than the precipitation of the nanospheres. Thereby, the growing COF film can retain its orientational growth induced by the flat FTO surface. In the case of the other COFs, precipitation likely occurs faster than the transmutation process. Consequently, while still crystalline COF films are growing, the fusing of the nanosphere to the film is unidirectional without any preferred orientation. Thus, the dynamic equilibrium between precipitation of the nanospheres and transmutation into the films would determine whether oriented layer-by-layer-like film growth is possible. ^{13}C CP-MAS solid-state NMR spectra confirmed the formation of the β-ketoenamine backbone in these thin films. ^{13}C CP-MAS SS spectra NMR exhibit the characteristic peaks of carbonyl carbons (–C=O) at ~184-182 ppm and exocyclic carbons (–C=C) at ~146-147 ppm. TpTta films exhibit signals at~168 ppm for the triazine ring carbons. TpEtBr films show signals at ~50.7 ppm for –CH_2– and 14.5 ppm for the –CH_3 carbons of ethyl groups (Figure 2h). SEM images of COF thin films showed that the surfaces are smooth and devoid of defects and cracks (Figure 2c-f). We have calculated the electronic properties of the COF thin films using HSE06 functional[24] in the FHI-Aims program[25] (Figure 3e and for further details see Section SI-10). The theoretical bandgaps of TpDPP, TpEtBr, TpTab, and TpTta COF thin films were calculated to be 2.01, 1.44, 2.30, and 2.34 eV (Figure 3e, S20). TpEtBr films have the lowest theoretical bandgap compared to other COF thin films. The lowest calculated bandgap and the visible in the valence and conduction bands indicate that the TpEtBr film should show a favourable semiconducting behaviour compared to the other investigated COF thin films. We performed UV-Vis spectroscopy and photoluminescence (PL) spectroscopies to investigate the optical properties of orientated COF films. The UV-vis spectra exhibit sharp absorption maxima at 464 nm for TpDPP, 446 nm for TpEtBr, 425 nm for TpTab, and 427 nm for TpTta (Figure 4a, 4b), respectively. We also compared the absorption maxima between the COF powders and oriented COF films. UV-vis DRS spectra of COF powders showed a broad absorption range at ~389-581 nm for TpDPP and 378-675 nm for TpEtBr (Figure S21). This may indicate the presence of crystallites with various crystalline domains and rather high defect densities in the COF powders. However, during the formation of COF thin

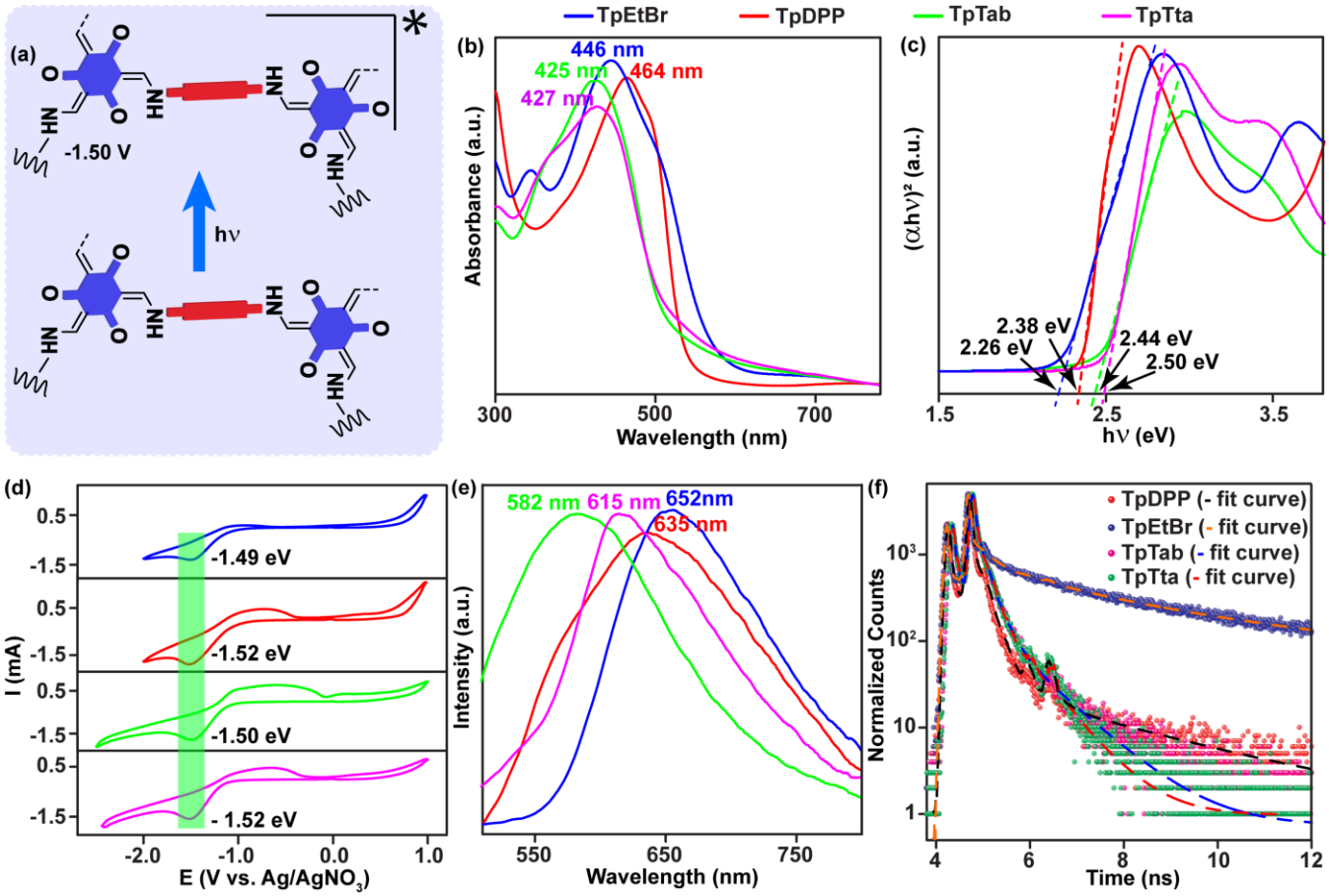

Figure 4. (a) Photoexcited state of COF backbone after irradiation of visible light. (b) UV-Vis spectra of COF thin films grown on the quartz surface. (c) Tauc plot analysis of COF thin films showing direct optical bandgaps. (d) Cyclic voltammograms of COF thin films in the presence of a nonaqueous electrolyte. (e) Photoluminescence (PL) spectra of COF thins films showing the emission maxima. The red, blue, green, and pink colored curves represent the TpDPP, TpEtBr, TpTab, and TpTta COF thin films in panels b-f. (f) TCSPC traces of all COF thin films were recorded at the respective emission maximum of each COF.

films the crystalline order increases and the defect density decreases, resulting in more defined optical absorption spectra. The measured optical (direct) band gap energies of TpDPP, TpEtBr, TpTab, and TpTta COF thin films are 2.38, 2.26, 2.44, and 2.50 eV, which is favourable for developing optoelectronic devices (Figure 4c). The optical bandgap energy trend of the four COF thin films matches well with their theoretical bandgap energy trend (cf. Figure 3e). The reduction potentials of TpDPP, TpEtBr, TpTab, and TpTta thin films measured using a cyclic voltammetric (CV) experiment were observed to be -1.49, -1.52, -1.52, and -1.50 V vs. $Ag/AgNO_3$. These reduction-potential values are attributed to the reduction of the COF backbone (Figure 4d). The conduction band energy (E_{CB}) of TpDPP, TpEtBr, TpTab, and TpTta were calculated to be -2.89, -2.91, -2.90 and -2.88 eV, respectively. The valance band energy (E_{VB}) was calculated to be -5.27 eV (TpDPP), -5.17 eV (TpEtBr), -5.34 eV (TpTab), and -5.38 eV (TpTta; detailed in Table S1). PL spectra demonstrated that upon excitation at 460 nm, TpDPP and TpEtBr thin films emit at 635 and 652 nm; the emission maxima of TpTab and TpTta COF appear at 582 and 615 nm upon excitation at 425 nm (Figure 4e). Due to better π-conjugation in the COF backbone and layers, the emission maxima of TpEtBr and TpDPP COFs are red-shifted by 53-70 nm and 20-37 nm, compared to the TpTab and TpTta COFs, respectively. We performed time-correlated single-photon counting (TCSPC) experiments to measure the excited state lifetimes of COF thin films. The decay curves of each thin film were fitted with three or four exponential components (Figure 4f). The average excited-state lifetime of the COF fluorophores was estimated to be 1.95 ns for TpDPP, 8.52 ns for TpEtBr, 0.58 ns for TpTab, and 0.15 ns for TpTta COF (Figure 4f, S22). The much longer lifetime of the TpEtBr COF indicates delayed recombination of photogenerated excitons, which is supported by the direct nature of the bandgap. In bilayer photodiode devices, such long-lived excitons are expected to yield large photocurrents under applied bias. Hence, TpEtBr COF is expected to be efficient for photogenerated charge separation. We equipped the above COF thin-film-coated devices with two sandwich electrodes for optoelectronic property measurements. To this end, we deposited a thin layer of TiO_2 on the patterned FTO surface and then deposited the COF thin film onto the TiO_2-coated FTO, where FTO acts as a transparent bottom electrode. To complete the device structure, we deposited Au thin layers on top of the COF thin film to serve as the top electrode. Hence, the complete architecture of the devices was glass/FTO/TiO_2/COF-film/Au. Current-voltage (*I-V* or *J-V* for current density) characteristics and the photo-sensitive

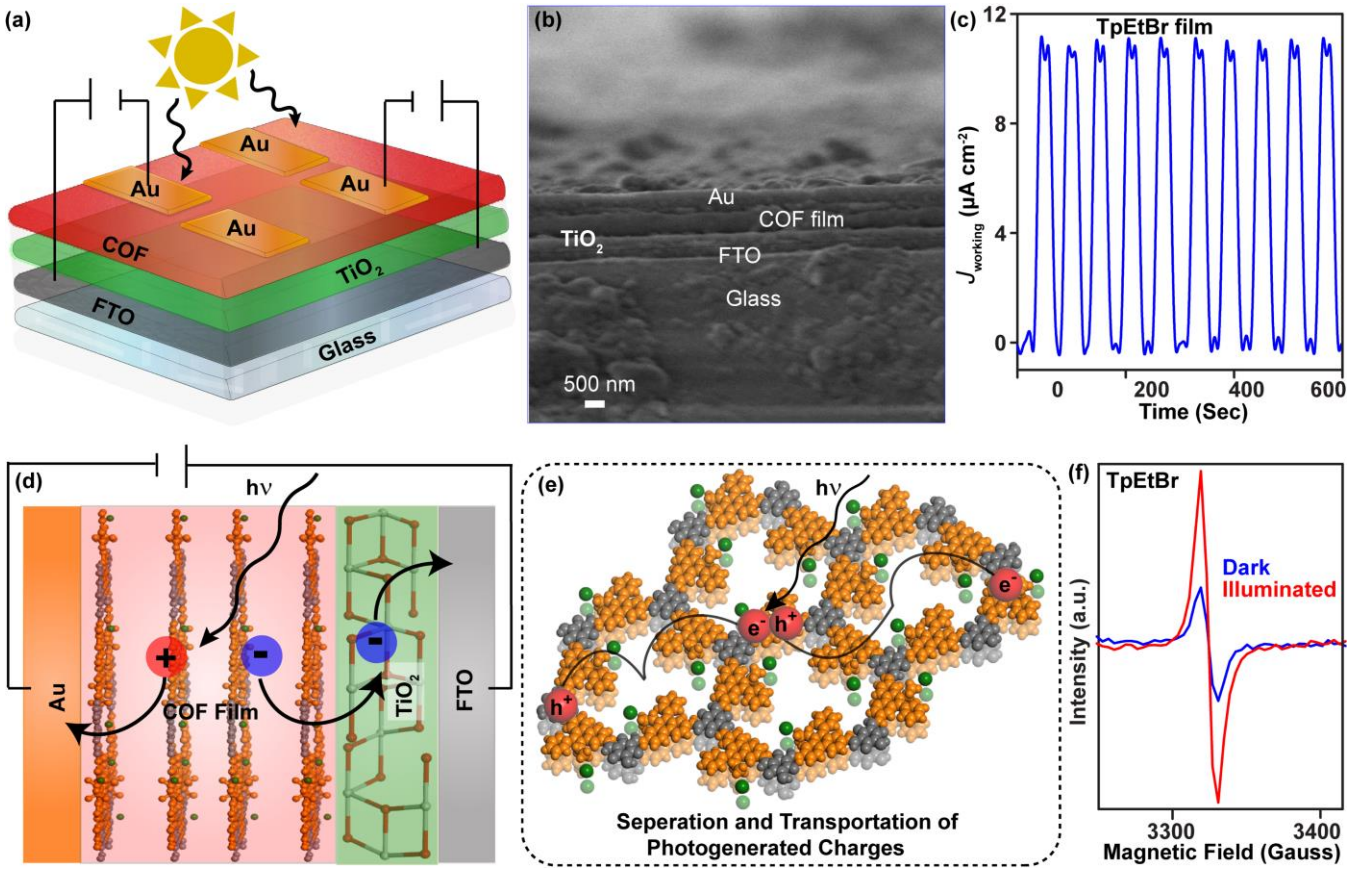

Figure 5. (a) Schematic representation of the device fabrication. (b) Cross-section SEM images of TpEtBr COF thin-film coated device. (c) Chronoamperometric photocurrent measurement of TpEtBr COF thin films with 30s interval without applying any external voltage. (d) Schematic representation of the mechanism of photocarrier generation in COF thin film sandwiched between the Au and FTO electrodes. (e) Schematic representation of separation and transportation of photogenerated charges (electrons and holes) through the COF pores and the layers. (f) Comparison of EPR spectra of TpEtBr COF thin films between dark and illuminated conditions.

conductivity changes in these devices were measured. (Figure 5a, S24). We used AM 1.5 G solar illumination with a power density of 100 mW cm^{-2} as a visible light source for the photo-excitation of the COF thin films. Based on the band alignment estimated from the above results (Figure 4c), COF layers that absorb the visible range of photons are expected to generate excitons and free charge carriers that can be extracted in the presence of applied bias. Thus, photogenerated free electrons from the conduction band of the COF thin film will be collected at the FTO electrode without much thermal loss, because of the favourable alignment of the conduction band of TiO_2 and FTO with that of the COF thin film. At the same time, the photogenerated hole carriers are collected at the Au electrode. The work function of gold is comparable to the valance band energy of COF thin films (Figure 5d, S25). Hence, FTO behaves as a cathode, and Au behaves as an anode. The thickness of TiO_2, COF thin films, and Au layers was determined to be 200, 300±20, and 100 nm by cross-sectional SEM measurement (Figure 5b, S35, S36). Under the zero applied bias, the observed current was extremely low under dark and illuminated conditions. This confirmed the binding energy of the charge-transfer excitons to be rather large. (Figure 5c, S26). This low current density manifested the charge separation and movement of charge throughout the COF backbone. The crystallinity, porosity, long-range order, and extended π- stacks in these COF thin films prevent, to some degree, the recombination of electron-hole pairs in the COF backbone. EPR spectroscopy was performed to confirm the separation of charges in the COF backbone under both dark and illuminated conditions. The EPR signal of these COF thin films appears at g = 2.00 in both dark and illuminated conditions. The peak intensity of COF films increases after irradiation with visible light. This observation indicates the slow recombination process of some fraction of the charge carriers (Figures 5e, 5f, and S23). The current density (*J*) was also measured as a function of applied voltage (*V*). The current density of the as-synthesized COF films was measured under dark and illuminated conditions in the potential range between -1.5 to +1.5 V. *J-V* curves of COF thin films showed photocurrent under illumination. The TpDPP, TpEtBr, TpTab, and TpTta COF thin films showed current densities of 1.7±0.18, 2.65±0.24, 0.0074±0.0002, and 0.028±0.006 mA cm^{-2} at 0.5 V under illuminated conditions at a steady-state AM 1.5G Solar Simulator. The current density of the TpEtBr thin film is 1.5, 95, and 358 times higher than that of the TpDPP, TpTta, and TpTab COF thin films, respectively (Figure 6a, S27). Therefore, the TpEtBr COF thin film emerged as the most efficient for light-induced charge separation among these four COF films. To measure the performance of these out-of-plane, photodetector devices, we measured their responsivity (R)

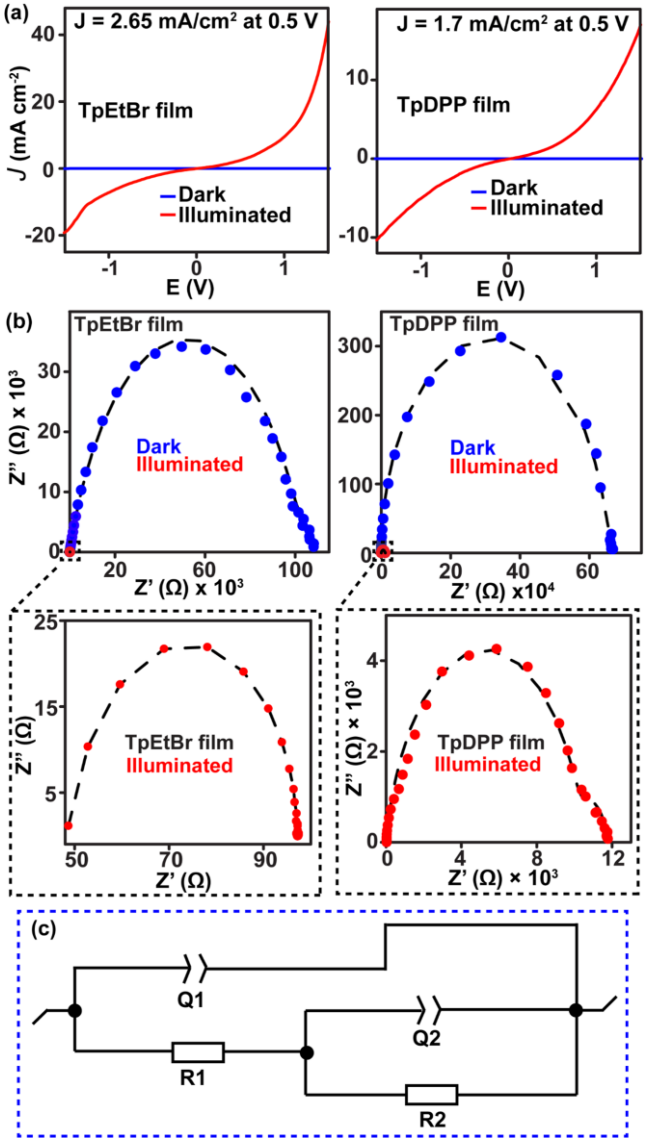

Figure 6. (a) *J-V* curves of TpEtBr, and TpDPP respectively, performed in the dark (blue) and under visible light illumination (red). (b) Electrochemical impedance spectroscopy (EIS) Nyquist plots of TpEtBr, TpDPP, TpTab, and TpTta COF thin films under dark (blue) and illuminated (red) conditions. (c) Fitted equivalence circuit of Nyquist plots of COF films under both dark and illuminated conditions.

and detectivity (D) values. We obtained the highest responsivity (R) and detectivity (D) of these devices at +1.5 V (Figure S28-30). The responsivity values were calculated to be 0.4387±0.002 AW^{-1} for TpEtBr, 0.1702±0.003 AW^{-1} for TpDPP, 0.0003±0.0001 AW^{-1} for TpTab, and 0.0011±0.0009 AW^{-1} for TpTta. The detectivity values were observed to be 0.794×10^{10} Jones for TpEtBr, 0.718×10^{10} Jones for TpDPP, 0.0025×10^{10} Jones for TpTab, and 0.0044×10^{10} Jones for TpTta. The R and D values follow the sequence of TpEtBr>TpDPP>TpTta>TpTab (Table S2 and figure S30). Nyquist plots were recorded under both dark and illuminated conditions to compare the charge-transfer resistance of COF thin films. The illuminated COF thin films generate smaller semicircles compared to the films placed in the dark (Figure 6b, 6c, S31-32). This observation demonstrates that illuminated COF thin films favor a higher photogenerated interfacial charge transfer than the films placed in the dark. The TpEtBr COF thin film shows a semicircle with the smallest diameter compared to the other three COF thin films, indicating the faster interfacial charge transfer rate of the TpEtBr COF thin film under illumination. We suggest that the near-degenerate alignment of the TpEtBr valence band and the Fermi energy of the Au electrode increases the probability of hole tunnelling, which lowers the carrier recombination and results in a higher photocurrent.[26] Hence, the TpEtBr film is efficient for electron-hole pair separation and shows the slowest recombination effect of photogenerated electron-hole pairs. To compare the hole mobility of all the COF films under dark and illuminated conditions, hole-only devices with the FTO/COF/Au architecture were prepared and the current-density of COF thin films in the dark and under illumination was measured (Figure S33, S34). Here, we considered that our devices have Ohmic contacts and that the charge-transport is a trap-free transport at a higher voltage. The measured current is the space-charge limited current (SCLC). We calculated the hole mobility of thin films using the Mott-Gurney equation

$$J = \frac{9}{8}\varepsilon_0\varepsilon_r\mu\frac{V^2}{L^3}$$

where J is the current density of the COF thin film obtained from the *J-V* measurement, ε_r is the dielectric constant of the COF calculated from the capacitance measurement, ε_0 is the permittivity of free space, L is the thickness of the COF layer obtained from cross-section SEM measurement, V is the voltage drop across the device, and μ is the hole mobility of thin films. We have measured the capacitance data of COF thin films to calculate their dielectric constant. The obtained capacitance data of COF thin films are 56 pf (TpDPP), 57 pf (TpEtBr), 55 pf (TpTab), and 57 pf (TpTta) (Table S3). Hence, the dielectric constants were calculated to be 2.11±0.12 for TpDPP, 2.14±0.1 for TpEtBr, 2.07±0.1 for TpTta, and 2.14±0.11 for TpTab COF thin films. These COF thin films grown on the TiO_2-coated FTO substrate and sandwiched between two electrodes afford high photocurrent and charge-carrier mobility after excitation with visible light with an intensity of 100 mW cm^{-2}. The illuminated hole mobility of 300±20 nm COF thin films was calculated to be $(8.15\pm0.64)\times10^{-3}$ cm^2 V^{-1} s^{-1} for TpEtBr, $(7.32\pm0.56)\times10^{-3}$ cm^2 V^{-1} s^{-1} for TpDPP, $(3.79\pm0.82)\times10^{-3}$ cm^2 V^{-1} s^{-1} for TpTab, and $(3.27\pm0.70)\times10^{-3}$ cm^2 V^{-1} s^{-1} for TpTta, which are higher in comparison with their dark hole-mobility (Table S4). These results establish the formation and migration of photoinduced holes with significant mobility in the COF backbones. The hole mobility of the COF thin films follows the sequence of TpEtBr>TpDPP>TpTab>TpTta. The TpEtBr film with the longest excited state lifetime shows the highest hole mobility among the COF thin films.

CONCLUSION

In conclusion, we have developed a unique sphere transmutation methodology to fabricate four porous, crystalline, and partially orientated COF thin films on 2×2 cm^2 TiO_2-coated FTO surfaces under reflux conditions.

This crystallization process results in continuous thin films with a uniform thickness of ~300±20 nm and low surface roughness. Crystallite domain sizes, nature of the grain boundaries, and type of layer assembly within the COF films are vital factors influencing light-induced charge migration. The energy correlation diagram of electrodes and COF thin films suggests that the COF thin film coated devices can serve as photodetectors. The COF backbone building units control the optoelectronic properties of these four COF thin films. We establish that the ionic TpEtBr COF has the lowest bandgap (2.26 eV) and longest excited state lifetime (~8.52 ns) of all investigated COF thin films. This makes the TpEtBr COF a favourable candidate for constructing a photodetector and an efficient material for charge-separation and -migration in the device. Accordingly, a photodetector device made with the charged TpEtBr COF thin film shows high photocurrent density (2.65±0.24 mA cm^{-2}) and hole mobility (8.15±0.64) × 10^{-3} cm^2 V^{-1} s^{-1} compared to devices made with the other COF thin films. A detailed investigation of the charge transport mechanism in these COF thin film coated devices is currently in progress.

Author Contributions

†S.B., H.S.S and S.P.C contributed equally to this work.

ASSOCIATED CONTENT

Supporting Information. Synthesis, crystallography, and characterization details are provided in the Supporting Information file. This material is available free of charge via the Internet at "http://pubs.acs.org".

AUTHOR INFORMATION

Corresponding Author
* sayanb@iiserkol.ac.in
* bein@lmu.de
* thomas.heine@tu-dresden.de
* r.banerjee@iiserkol.ac.in

ORCID

Rahul Banerjee: 0000-0002-3547-4746
Thomas Heine: 0000-0003- 2379-6251
Thomas Bein: 0000-0001-7248-5906
Sayan Bhattacharyya: 0000-0001-8074-965X
Thalasseril G. Ajithkumar: 0000-0002-9217-2138
Ratheesh K Vijayaraghavan: 0000-0001-8952-8087
Ankita Shelke: 0000-0001-6596-487X
Yingying Zhang: 0000-0003-2135-3799
Miroslav Položij: 0000-0002-3016-9523
Agnieszka Kuc: 0000-0002-9458-4136
Dominic Blätte: 0000-0003-4030-6330
Roman Guntermann: 0000-0003-3617-0768
Kaushik Dey: 0000-0003-4889-8035
Sonu Pratap Chaudhary: 0000-0002-3300-3019
Himadri Sekhar Sasmal: 0000-0001-7355-8783
Saikat Bag: 0000-0002-0464-2276

Notes

The authors declare no competing financial interests.

ACKNOWLEDGMENT

S.B. and S.P.C. acknowledge CSIR for a Research Fellowship. H.S.S. acknowledges DST-SERB, India, for a RA Fellowship [CRG/2018/000314]. K.D. acknowledges DST-SERB, India, for a RA Fellowship [(CRG/ 2018/000314]. R.B. acknowledges a SwarnaJayanti Fellowship grant [DST/SJF/CSA-02/2016-2017], DST Mission Innovation [DST/TM/EWO/MI/CCUS/17 and DST/TMD(EWO)/IC5-2018/01(C)], and DST SERB [CRG/2018/000314] for funding. R.B. and T.B also acknowledge a Carl Friedrich von Siemens Research Fellowship and the Alexander von Humboldt Foundation for a research stay at Ludwig- Maximilians Universität (LMU) in München, Germany. S.Bh. thanks SERB for funding under Sanction No. CRG/2020/000084 and STR/2021/000001. T.B. acknowledges support from the Center for NanoScience Munich (CeNS) and the Bavarian research network Solar Technologies go Hybrid (SolTech), as well as funding from the Deutsche Forschungsgemeinschaft (DFG, German Research Foundation) under Germany´s Excellence Strategy – EXC 2089/1 – 390776260. Y.Z. acknowledges the China Scholarship Council. M.P. acknowledges the Saxonian Ministry for Science and Art (DCC F-012177-701-XD0-1030602) for funding. Y.Z., M.P., A.K., and T.H. acknowledge ZIH Dresden for computer time. Y.Z., A.K. and T.H. acknowledge Deutsche Forschungsgemeinschaft for support within CRC 1415 and SPP2244. We acknowledge Mr. R. B. Amal Raj and E. Bhoje Gowd for helping in PXRD data collection.

REFERENCES

1. (a) Yaghi, O.M.; Keeffe, M.O.; Ockwig, N.W.; Chae, H.K.; Eddaoudi, M.; Kim, J. Reticular synthesis and the design of new materials. *Nature* **2003**, 423, 705-714. (b) Zhao, Y.; Guo, L.; Gandara, F.; Ma, Y.; Liu, Z.; Zhu, C.; Lyu, H.; Trickett, C. A.; Kapustin, E. A.; Terasaki, O.; Yaghi, O.M. A Synthetic Route for Crystals of Woven Structures, Uniform Nanocrystals, and Thin Films of Imine Covalent Organic Frameworks. *J. Am. Chem. Soc*. **2017**, 139, 13166-13172. (c) Ji, Z.; Li, T.; Yaghi, O. M. Sequencing of metals in multivariate metal-organic frameworks. *Science* **2020**, 369, 674–780. (d) Côte, A. P.; Benin, A. I.; Ockwig, N. W.; O'Keeffe, M.; Matzger, A. J.; Yaghi, O. M. Porous, Crystalline, Covalent Organic Frameworks. *Science* **2005**, 310, 1166–1170. (e) Nguyen, H. L.; Gropp, C.; Ma, Y.; Zhu, C.; Yaghi, O. M.; 3D Covalent Organic Frameworks Selectively Crystallized through Conformational Design. *J. Am. Chem. Soc*. **2020**, 142, 20335-20339. (f) Cai, S. L.; Zhang, Y. B.; Pun, A. B.; He, B.; Yang, J.; Toma, F. M.; Sharp, I. D.; Yaghi, O. M.; Fan, J.; Zheng, S. R.; Zhang, W. G.; Liu, Y. Tunable electrical conductivity in oriented thin films of tetrathiafulvalene-based covalent organic framework. *Chem. Sci*. **2014**, 5, 4693–4700.
2. (a) Kandambeth, S.; Dey, K.; Banerjee, R. Covalent Organic Frameworks: Chemistry beyond the Structure. *J. Am. Chem. Soc*. **2019**, 141, 1807-1822. (b) Kandambeth, S.; Venkatesh, V.; Shinde, B. D.; Kumari, S.; Halder, A.; Verma, S.; Banerjee, R. Self-templated chemically stable hollow spherical covalent organic framework. *Nature Communications* **2015**, 6, 6786. (c) Sasmal, H. S.; Halder, A.; Kunjattu H, S.; Kaushik Dey, K.; Nadol, A.; Ajithkumar, A. T.; Prachiti Ravindra Bedadur, P. R.; Banerjee, R. Covalent Self-Assembly in Two Dimensions: Connecting Covalent Organic Framework Nanospheres into Crystalline and Porous Thin Films. *J. Am. Chem. Soc*. **2019**, 141, 20371-20379. (d) Dey, K.; Pal, M.; Rout, K. C.; Kunjattu H, S.; Das, A.; Mukherjee, R.; Kharul, U. K.; Banerjee, R. Selective Molecular Separation by Interfacially Crystallized Covalent Organic Framework Thin Films. *J. Am. Chem. Soc*. **2017**, 139, 13083-13091. (e) Dey, K.; Mohata, S.; Banerjee, R. Covalent Organic Frameworks and Supramolecular Nano-Synthesis.

ACS Nano **2021**, 15, 8, 12723–12740. (f) Halder, A.; Karak, S.; Addicoat, M.; Bera, S.; Chakraborty, A.; Kunjattu, S. H.; Pachfule, P.; Heine, T.; Banerjee, R. Ultra-stable Imine-based Covalent Organic Frameworks for Sulfuric acid Recovery: An Effect of Interlayer Hydrogen Bonding. *Angew. Chem. Int. Ed.* **2018**, 57, 5797.

3. (a)Banerjee, T.; Gottschling, K.; Savasci, G.; Ochsenfeld, C.; Lotsch, B. V., H_2 Evolution with Covalent Organic Framework Photocatalysts. *ACS Energy Lett.* **2018,** *3*, 400-409. (b) Banerjee, T.; Haase, F.; Savasci, G.; Gottschling, K.; Ochsenfeld, C.; Lotsch, B. V., Single-Site Photocatalytic H2 Evolution from Covalent Organic Frameworks with Molecular Cobaloxime Co-Catalysts. *J. Am. Chem. Soc.* **2017,** *139*, 16228-16234. (c) Bessinger, D.; Muggli, K.; Beetz, M.; Auras, F.; Bein, T., Fast-Switching Vis-IR Electrochromic Covalent Organic Frameworks. *J. Am. Chem. Soc.* **2021,** *143*, 7351-7357. (d) Bi, S.; Yang, C.; Zhang, W.; Xu, J.; Liu, L.; Wu, D.; Wang, X.; Han, Y.; Liang, Q.; Zhang, F., Two-dimensional semiconducting covalent organic frameworks via condensation at arylmethyl carbon atoms. *Nat. Commun.* **2019,** *10*, 2467.
4. (a) Aiyappa, H. B.; Thote, J.; Shinde, D. B.; Banerjee, R.; Kurungot, S., Cobalt-Modified Covalent Organic Framework as a Robust Water Oxidation Electrocatalyst. *Chemistry of Materials* **2016,** *28*, 4375-4379. (b) Chandra, S.; Roy Chowdhury, D.; Addicoat, M.; Heine, T.; Paul, A.; Banerjee, R., Molecular Level Control of the Capacitance of Two-Dimensional Covalent Organic Frameworks: Role of Hydrogen Bonding in Energy Storage Materials. *Chemistry of Materials* **2017,** *29*, 2074-2080. (c) Halder, A.; Ghosh, M.; Khayum, M. A.; Bera, S.; Addicoat, M.; Sasmal, H. S.; Karak, S.; Kurungot, S.; Banerjee, R., Interlayer Hydrogen-Bonded Covalent Organic Frameworks as High-Performance Supercapacitors. *J. Am. Chem. Soc.* **2018,** *140*, 10941-10945. (d) Khayum, M. A.; Vijayakumar, V.; Karak, S.; Kandambeth, S.; Bhadra, M.; Suresh, K.; Acharambath, N.; Kurungot, S.; Banerjee, R., Convergent Covalent Organic Framework Thin Sheets as Flexible Supercapacitor Electrodes. *ACS Appl. Mater. Interfaces* **2018,** *10*, 28139-28146. (e) Mohammed, A. K.; Vijayakumar, V.; Halder, A.; Ghosh, M.; Addicoat, M.; Bansode, U.; Kurungot, S.; Banerjee, R., Weak Intermolecular Interactions in Covalent Organic Framework-Carbon Nanofiber Based Crystalline yet Flexible Devices. *ACS Appl. Mater. Interfaces* **2019,** *11*, 30828-30837. (f) Mukherjee, G.; Thote, J.; Aiyappa, H. B.; Kandambeth, S.; Banerjee, S.; Vanka, K.; Banerjee, R., A porous porphyrin organic polymer (PPOP) for visible light triggered hydrogen production. *Chem. Commun.* **2017,** *53*, 4461-4464.
5. (a) Li, Y.; Chen, Q.; Xu, T.; Xie, Z.; Liu, J.; Yu, X.; Ma, S.; Qin, T.; Chen, L., De Novo Design and Facile Synthesis of 2D Covalent Organic Frameworks: A Two-in-One Strategy. *J. Am. Chem. Soc.* **2019,** *141*, 13822-13828. (b) Medina, D. D.; Petrus, M. L.; Jumabekov, A. N.; Margraf, J. T.; Weinberger, S.; Rotter, J. M.; Clark, T.; Bein, T., Directional Charge-Carrier Transport in Oriented Benzodithiophene Covalent Organic Framework Thin Films. *ACS Nano.* **2017,** *11*, 2706-2713. (c) Medina, D. D.; Sick, T.; Bein, T., Photoactive and Conducting Covalent Organic Frameworks. *Advanced Energy Materials* **2017,** *7*, 1700387.
6. (a) Stegbauer, L.; Schwinghammer, K.; Lotsch, B. V., A hydrazone-based covalent organic framework for photocatalytic hydrogen production. *Chem. Sci.* **2014,** *5*, 2789-2793. (b) T Sick, T.; Hufnagel, A. G.; Kampmann, J.; Kondofersky, I.; Calik, M.; Rotter, J. M.; Evans, A.; Doblinger, M.; Herbert, S.; Peters, K.; Bohm, D.; Knochel, P.; Medina, D. D.; Fattakhova-Rohlfing, D.; Bein, T., Oriented Films of Conjugated 2D Covalent Organic Frameworks as Photocathodes for Water Splitting. *J. Am. Chem. Soc.* **2018,** *140*, 2085-2092.
7. (a) Vyas, V. S.; Haase, F.; Stegbauer, L.; Savasci, G.; Podjaski, F.; Ochsenfeld, C.; Lotsch, B. V., A tunable azine covalent organic framework platform for visible light-induced hydrogen generation. *Nat. Commun.* **2015,** *6*, 8508. (b) Wan, S.; Gándara, F.; Asano, A.; Furukawa, H.; Saeki, A.; Dey, S. K.; Liao, L.; Ambrogio, M. W.; Botros, Y. Y.; Duan, X.; Seki, S.; Stoddart, J. F.; Yaghi, O. M., Covalent Organic Frameworks with High Charge Carrier Mobility. *Chemistry of Materials* **2011,** *23*, 4094-4097.
8. Wang, Z.; Walter, L. S.; Wang, M.; Petkov, P. S.; Liang, B.; Qi, H.; Nguyen, N. N.; Hambsch, M.; Zhong, H.; Wang, M.; Park, S.; Renn, L.; Watanabe, K.; Taniguchi, T.; Mannsfeld, S. C. B.; Heine, T.; Kaiser, U.; Zhou, S.; Weitz, R. T.; Feng, X.; Dong, R., Interfacial Synthesis of Layer-Oriented 2D Conjugated Metal-Organic Framework Films toward Directional Charge Transport. *J. Am. Chem. Soc.* **2021,** *143*, 13624-13632.
9. (a) Wei, S.; Zhang, F.; Zhang, W.; Qiang, P.; Yu, K.; Fu, X.; Wu, D.; Bi, S.; Zhang, F., Semiconducting 2D Triazine-Cored Covalent Organic Frameworks with Unsubstituted Olefin Linkages. *J. Am. Chem. Soc.* **2019,** *141*, 14272-14279. (b) Xing, G.; Zheng, W.; Gao, L.; Zhang, T.; Wu, X.; Fu, S.; Song, X.; Zhao, Z.; Osella, S.; Martinez-Abadia, M.; Wang, H. I.; Cai, J.; Mateo-Alonso, A.; Chen, L., Nonplanar Rhombus and Kagome 2D Covalent Organic Frameworks from Distorted Aromatics for Electrical Conduction. *J. Am. Chem. Soc.* **2022,** *144*, 5042-5050. Conduction. *J. Am. Chem. Soc.* **2022,** *144*, 5042-5050.
10. (a) Zhai, L.; Wei, W.; Ma, B.; Ye, W.; Wang, J.; Chen, W.; Yang, X.; Cui, S.; Wu, Z.; Soutis, C.; Zhu, G.; Mi, L., Cationic Covalent Organic Frameworks for Fabricating an Efficient Triboelectric Nanogenerator. *ACS Materials Letters* **2020,** *2*, 1691-1697. (b) Zhang, Y.; Položij, M.; Heine, T., Statistical Representation of Stacking Disorder in Layered Covalent Organic Frameworks. *Chemistry of Materials* **2022,** *34*, 2376-2381. Brus, V. V.; Kyaw, A. K. K.; Maryanchuk, P. D.; Zhang, J., Quantifying interface states and bulk defects in high-efficiency solution-processed small-molecule solar cells by impedance and capacitance characteristics. *Progress in Photovoltaics: Research and Applications* **2015,** *23,* 1526-1535.
11. (a) Calik, M.; Auras, F.; Salonen, L. M.; Bader, K.; Grill, I.; Handloser, M.; Medina, D. D.; Dogru, M.; Lobermann, F.; Trauner, D.; Hartschuh, A.; Bein, T., Extraction of photogenerated electrons and holes from a covalent organic framework integrated heterojunction. *J. Am. Chem. Soc.* **2014,** *136*, 17802-7. (b) Chen, X.; Addicoat, M.; Jin, E.; Zhai, L.; Xu, H.; Huang, N.; Guo, Z.; Liu, L.; Irle, S.; Jiang, D., Locking covalent organic frameworks with hydrogen bonds: general and remarkable effects on crystalline structure, physical properties, and photochemical activity. *J. Am. Chem. Soc.* **2015,** *137*, 3241-7. (c) Dogru, M.; Handloser, M.; Auras, F.; Kunz, T.; Medina, D.; Hartschuh, A.; Knochel, P.; Bein, T., A photoconductive thienothiophene-based covalent organic framework showing charge transfer towards included fullerene. *Angew. Chem. Int. Ed.* **2013,** *52*, 2920-4. (d) Feng, T.; Streater, D.; Sun, B.; Duisenova, K.; Wang, D.; Liu, Y.; Huang, J.; Zhang, J., Tuning Photoexcited Charge Transfer in Imine-Linked Two-Dimensional Covalent Organic Frameworks. *J. Phys. Chem. Lett.* **2022,** *13*, 1398-1405. (e) Gao, B.; Yu, X.; Wang, T.; Gong, H.; Fan, X.; Xue, H.; Jiang, C.; Chang, K.; Huang, X.; He, J., Promoting charge separation by rational integration of a covalent organic framework on a BiVO4 photoanode. *Chem. Commun.* **2022,** *58*, 1796-1799.
12. (a) Ghosh, S.; Tsutsui, Y.; Kawaguchi, T.; Matsuda, W.; Nagano, S.; Suzuki, K.; Kaji, H.; Seki, S., Band-like Transport of Charge Carriers in Oriented Two-Dimensional Conjugated Covalent Organic Frameworks. *Chemistry of Materials* **2022,** *34*, 736-745. (b) Gunther, M.; Blatte, D.; Oechsle, A. L.; Rivas, S. S.; Yousefi Amin, A. A.; Muller-Buschbaum, P.; Bein, T.; Ameri, T., Increasing Photostability of Inverted Nonfullerene Organic Solar Cells by Using Fullerene Derivative Additives. *ACS Appl. Mater. Interfaces* **2021,** *13*, 19072-19084. (c) Guo, J.; Xu, Y.; Jin, S.; Chen, L.; Kaji, T.; Honsho, Y.; Addicoat, M. A.; Kim, J.; Saeki, A.; Ihee, H.; Seki, S.; Irle, S.; Hiramoto, M.; Gao, J.; Jiang, D.,

Conjugated organic framework with three-dimensionally ordered stable structure and delocalized pi clouds. *Nat. Commun.* **2013,** *4*, 2736. (d) Hao, Q.; Li, Z. J.; Bai, B.; Zhang, X.; Zhong, Y. W.; Wan, L. J.; Wang, D., A Covalent Organic Framework Film for Three-State Near-Infrared Electrochromism and a Molecular Logic Gate. *Angew. Chem. Int. Ed.* **2021,** *60*, 12498-12503. (e) Hao, Q.; Li, Z. J.; Lu, C.; Sun, B.; Zhong, Y. W.; Wan, L. J.; Wang, D., Oriented Two-Dimensional Covalent Organic Framework Films for Near-Infrared Electrochromic Application. *J. Am. Chem. Soc.* **2019,** *141*, 19831-19838. (f) He, S.; Rong, Q.; Niu, H.; Cai, Y., Construction of a superior visible-light-driven photocatalyst based on a C3N4 active centre-photoelectron shift platform-electron withdrawing unit triadic structure covalent organic framework. *Chem. Commun.* **2017,** *53*, 9636-9639.

13. (a) Medina, D. D.; Rotter, J. M.; Hu, Y.; Dogru, M.; Werner, V.; Auras, F.; Markiewicz, J. T.; Knochel, P.; Bein T. Room Temperature Synthesis of Covalent-Organic Framework Films through Vapor-Assisted Conversion. *J. Am. Chem. Soc*. **2015**, 137, 1016-1019. (b) Chen, Y.; Cui, H.; Zhang, J.; Zhao, K.; Ding, D.; Guo, J.; Li, L.; Tian, Z.; Tang, Z. Surface growth of highly oriented covalent organic framework thin film with enhanced photoresponse speed. *RSC Adv*. **2015**, 5, 92573–92576. (c) M. Rotter, J. M.; Weinberger, S.; Kampmann, J.; Sick, T.; Shalom, M.; Bein, T.; Medina, D. D. Covalent Organic Framework Films through Electrophoretic Deposition-Creating Efficient Morphologies for Catalysis. *Chem. Mater*. **2019**, 31, 10008-10016. (d) Wang, H.; Zeng, Z.; Xu, P.; Li, L.; Zeng, G.; Xiao, R.; Tang, Z.; Huang, D.; Tang, L.; Lai, C.; Jiang, D.; Liu, Y.; Yi, H.; Qin, L.; Ye, S.; Ren, X.; Tang, W. Recent progress in covalent organic framework thin films: fabrications, applications and perspectives. *Chem. Soc. Rev*. **2019**, 48, 488-516. (e) Zhao, X.; Pachfule, P.; Thomas, A. Covalent organic frameworks (COFs) for electrochemical applications. *Chem. Soc. Rev.*, **2021**, 50, 6871.
14. (a) Shinde, D. B.; Sheng, G.; Li, X.; Ostwal, M.; Emwas, A. H.; Huang, K. W.; Lai, Z. Crystalline 2D Covalent Organic Framework Membranes for HighFlux Organic Solvent Nanofiltration. *J. Am. Chem. Soc*. **2018**, 140, 14342-14349. (b) Zhou, D.; Tan, X.; Wu, H.; Tian, L.; Li, M. Synthesis of C-C Bonded Two-Dimensional Conjugated Covalent Organic Framework Films by Suzuki Polymerization on a Liquid–Liquid Interface. *Angew. Chem. Int. Ed*. **2019**, 58, 1376 –1381. (c) Liu, J.; Han, G.; Zhao, D.; Lu, K.; Gao, J.; Chung, T.S. Self-standing and flexible covalent organic framework (COF) membranes for molecular separation. *Sci. Adv*. **2020**, 6, 41. (c) Sahabudeen, H.; Qi, H.; Ballabio, M.; Položij, M.; Olthof, S.; Shivhare, R.; Jing, Y.; Park, S.; Liu, K.; Zhang, T.; Ma, J.; Rellinghaus, B.; Mannsfeld, S.; Heine, T.; Bonn, M.; Cánovas, E.; Zheng, Z.; Kaiser, U.; Dong, R.; Feng, X. Highly Crystalline and emiconducting Imine-Based Two-Dimensional Polymers Enabled by Interfacial Synthesis. *Angew. Chem. Int. Ed*. **2020**, 59, 6028 – 6036.
15. (a) Rotter, J. M.; Guntermann, R.; Auth, M.; Mahringer, A.; Sperlich, A.; Dyakonov, V.; Medina, D. D.; Bein, T., Highly conducting Wurster-type twisted covalent organic frameworks. *Chem. Sci.* **2020,** *11*, 12843-12853. (b) Sick, T.; Hufnagel, A. G.; Kampmann, J.; Kondofersky, I.; Calik, M.; Rotter, J. M.; Evans, A.; Doblinger, M.; Herbert, S.; Peters, K.; Bohm, D.; Knochel, P.; Medina, D. D.; Fattakhova-Rohlfing, D.; Bein, T., Oriented Films of Conjugated 2D Covalent Organic Frameworks as Photocathodes for Water Splitting. *J. Am. Chem. Soc.* **2018,** *140*, 2085-2092.
16. (a) Jin, E.; Geng, K.; Fu, S.; Addicoat, M. A.; Zheng, W.; Xie, S.; Hu, J. S.; Hou, X.; Wu, X.; Jiang, Q.; Xu, Q. H.; Wang, H. I.; Jiang, D., Module-Patterned Polymerization towards Crystalline 2D sp^2-Carbon Covalent Organic Framework Semiconductors. *Angew. Chem. Int. Ed.* **2022,** *61*, e202115020. (b) Jin, S.; Ding, X.; Feng, X.; Supur, M.; Furukawa, K.; Takahashi, S.; Addicoat, M.; El-Khouly, M. E.; Nakamura, T.; Irle, S.; Fukuzumi, S.; Nagai, A.; Jiang, D., Charge dynamics in a donor-acceptor covalent organic framework with periodically ordered bicontinuous heterojunctions. *Angew. Chem. Int. Ed.* **2013,** *52*, 2017-21. (C) Lau, V. W. h.; Lotsch, B. V., A Tour-Guide through Carbon Nitride-Land: Structure- and Dimensionality-Dependent Properties for Photo (Electro)Chemical Energy Conversion and Storage. *Advanced Energy Materials* **2021,** *12*, 2101078.
17. (a) Le Corre, V. M.; Duijnstee, E. A.; El Tambouli, O.; Ball, J. M.; Snaith, H. J.; Lim, J.; Koster, L. J. A., Revealing Charge Carrier Mobility and Defect Densities in Metal Halide Perovskites via Space-Charge-Limited Current Measurements. *ACS Energy Lett.* **2021,** *6*, 1087-1094. (b) Duijnstee, E. A.; Ball, J. M.; Le Corre, V. M.; Koster, L. J. A.; Snaith, H. J.; Lim, J., Toward Understanding Space-Charge Limited Current Measurements on Metal Halide Perovskites. *ACS Energy Letters* **2020,** *5*, 376-384.
18. (a) Teuscher, J.; Brauer, J. C.; Stepanov, A.; Solano, A.; Boziki, A.; Chergui, M.; Wolf, J. P.; Rothlisberger, U.; Banerji, N.; Moser, J. E., Charge separation and carrier dynamics in donor-acceptor heterojunction photovoltaic systems. *Struct. Dyn.* **2017,** *4*, 061503. (b) Wang, S.; Wang, X.; Yao, B.; Zhang, B.; Ding, J.; Xie, Z.; Wang, L., Solution-Processed Phosphorescent Organic Light-Emitting Diodes with Ultralow Driving Voltage and Very High-Power Efficiency. *Sci. Rep.* **2015,** *5*, 12487. Yuan, S.; Peng, J.; Cai, B.; Huang, Z.; Garcia-Esparza, A. T.; Sokaras, D.; Zhang, Y.; Giordano, L.; Akkiraju, K.; Zhu, Y. G.; Hubner, R.; Zou, X.; Roman-Leshkov, Y.; Shao-Horn, Y., Tunable metal hydroxide-organic frameworks for catalysing oxygen evolution. *Nat. Mater.* **2022**.
19. (a) Facchetti, A. Pi-Conjugated Polymers for Organic Electronics and Photovoltaic Cell Applications. *Chem. Mater.* **2011,** *23*, 733–758. (b) Mishra, A.; Bauerle, P. Small Molecule Organic Semiconductors on the Move: Promises for Future Solar Energy Technology. *Angew. Chem., Int. Ed.* **2012,** *51,* 2020–2067. (c) Ding, X.; Guo, J.; Feng, X.; Honsho, Y.; Guo, J.; Seki, S.; Maitarad, P.; Saeki, A.; Nagase, S.; Jiang, D. Synthesis of Metallophthalocyanine Covalent Organic Frameworks that Exhibit High Carrier Mobility and Photoconductivity. *Angew. Chem., Int. Ed.* **2011,** *50*, 1289–93. (d) Snaith, H. J.; Gratzel, M. Light-Enhanced Charge Mobility in a Molecular Hole Transporter. *Phys. Rev. Lett.* **2007**, *98,* 177402. (e) Koole, M.; Frisenda, R.; Petrus, M. L.; Perrin, M. L.; van der Zant, H. S. J.; Dingemans, T. J. Charge Transport Through Conjugated Azomethine-Based Single Molecules for Optoelectronic Applications. *Org. Electron.* **2016,** *34,* 38–41. (f) Blom, P. W. M.; Tanase, C.; de Leeuw, D. M.; Coehoorn, R. Thickness Scaling of the Space-Charge-Limited Current in Poly (pPhenylene Vinylene). *Appl. Phys. Lett.* **2005,** *86,* 92105.
20. Elstner M.; Porezag, D.; Jungnickel, G.; Elsner, J.; Haugk, M.; Frauenheim, T.; Suhai, S.; Seifert, G. *Phys. Rev. B.* **1998**, *58*, 7260-7268.
21. Gaus, M.; Goez, A.; Elstner M. J. Chem. Theory Comput., **2013**, *9*, 338-354.
22. Rüger, R.; Yakovlev, A.; Philipsen, P.; Borini, S.; Melix, P.; Oliveira, A.F.; Franchini, M.; van Vuren, T.; Soini, T.; de Reus, M.; Ghorbani Asl, M.; Teodoro, T. Q.; McCormack, D.; Patchkovskii, S.; Heine T. AMS DFTB 2021, SCM, Theoretical Chemistry, Vrije Universiteit, Amsterdam, The Netherlands, http://www.scm.com.
23. Zhang, Y.; Polozij, M.; Heine, T. Chem. Mater. **2022**, *34*, 2376–2381.
24. J. Heyd, G. E. Scuseria, M. Ernzerhof, *The Journal of Chemical Physics* **2003**, *118*, 8207--8215; J. Heyd, G. E. Scuseria, M. Ernzerhof, *The Journal of Chemical Physics* **2006**, *124*, 219906.
25. V. Blum, R. Gehrke, F. Hanke, P. Havu, V. Havu, X. Ren, K. Reuter, M. Scheffler, *Computer Physics Communications* **2009**, *180*, 2175-2196.

26. Ghosh, D; Ghosh, A; Ali, M. Y; Bhattacharyya, S. Photoactive Core–Shell Nanorods as Bifunctional Electrodes for Boosting the Performance of Quantum Dot Sensitized Solar Cells and Photoelectrochemical Cells. *Chem. Mater.* **2018,** *30,* 6071–6081.

Table of Contents

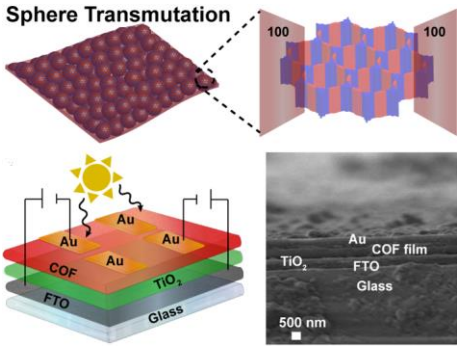

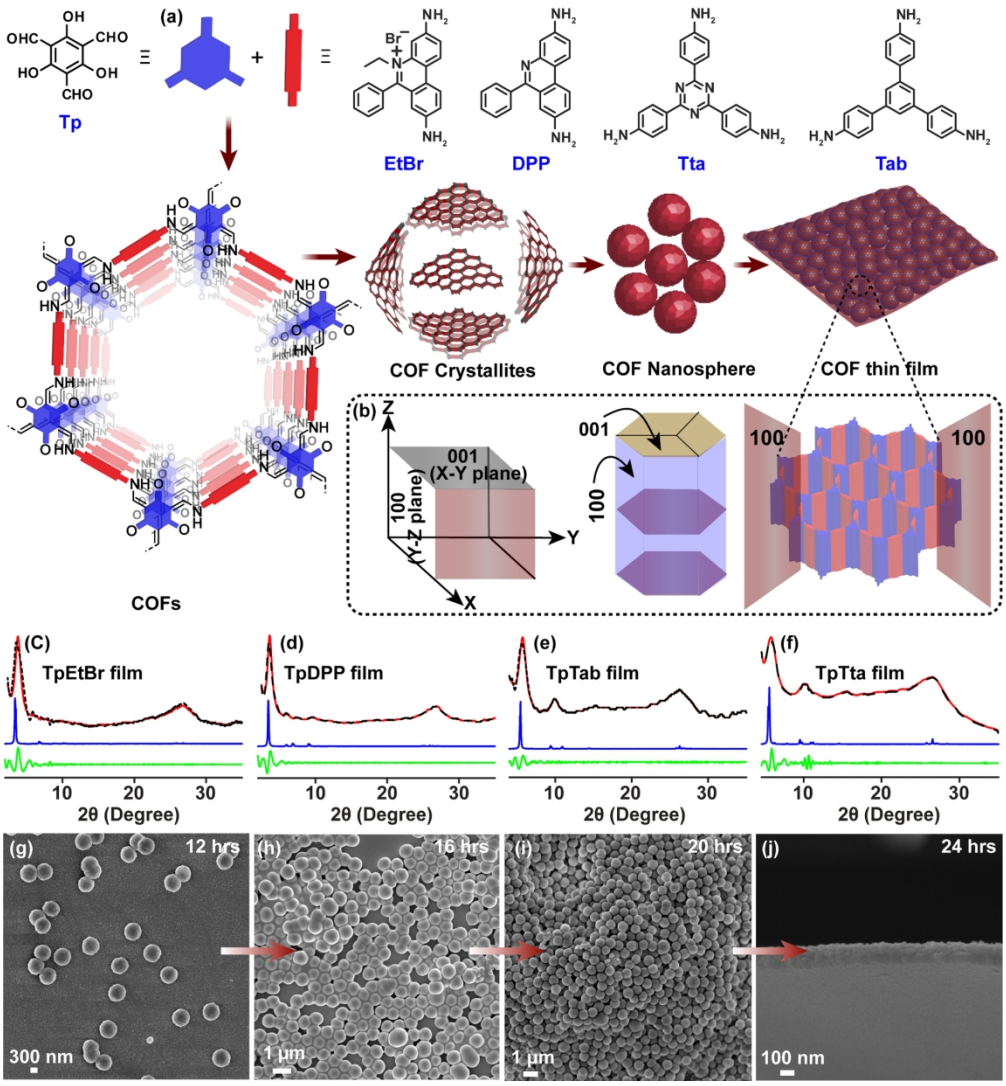

Figure 1

177x190mm (300 x 300 DPI)

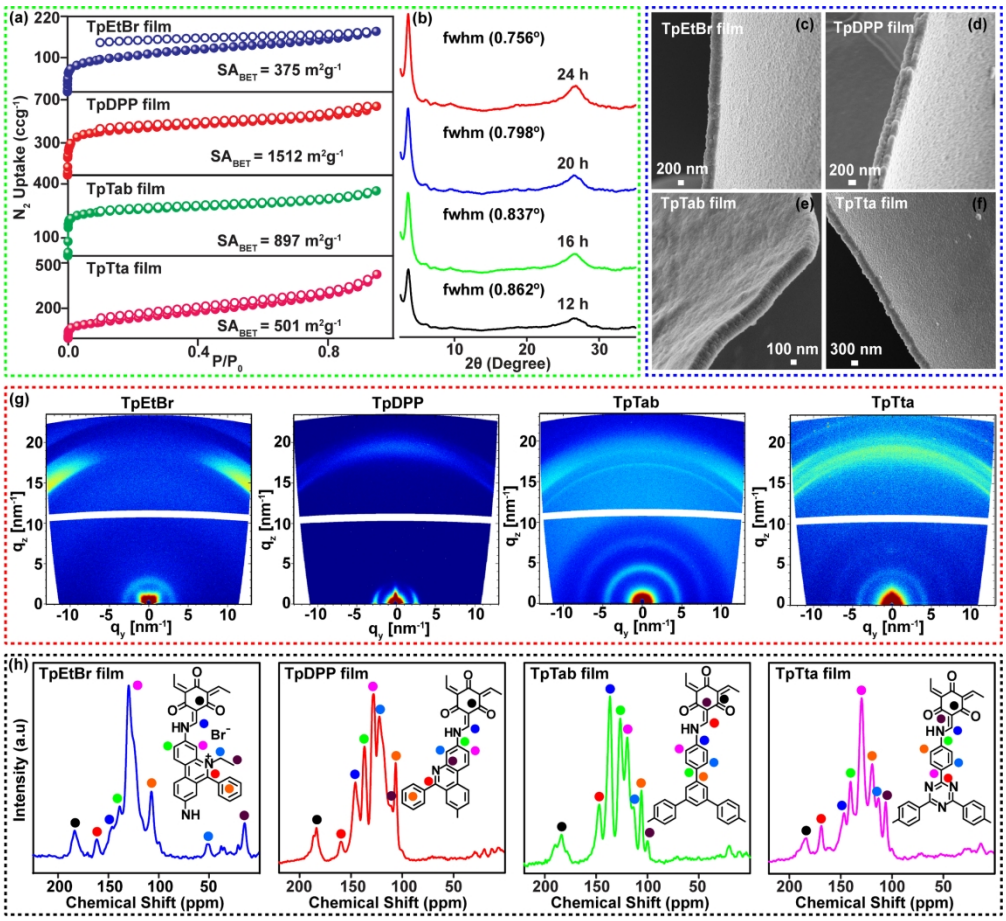

Figure 2

209x190mm (300 x 300 DPI)

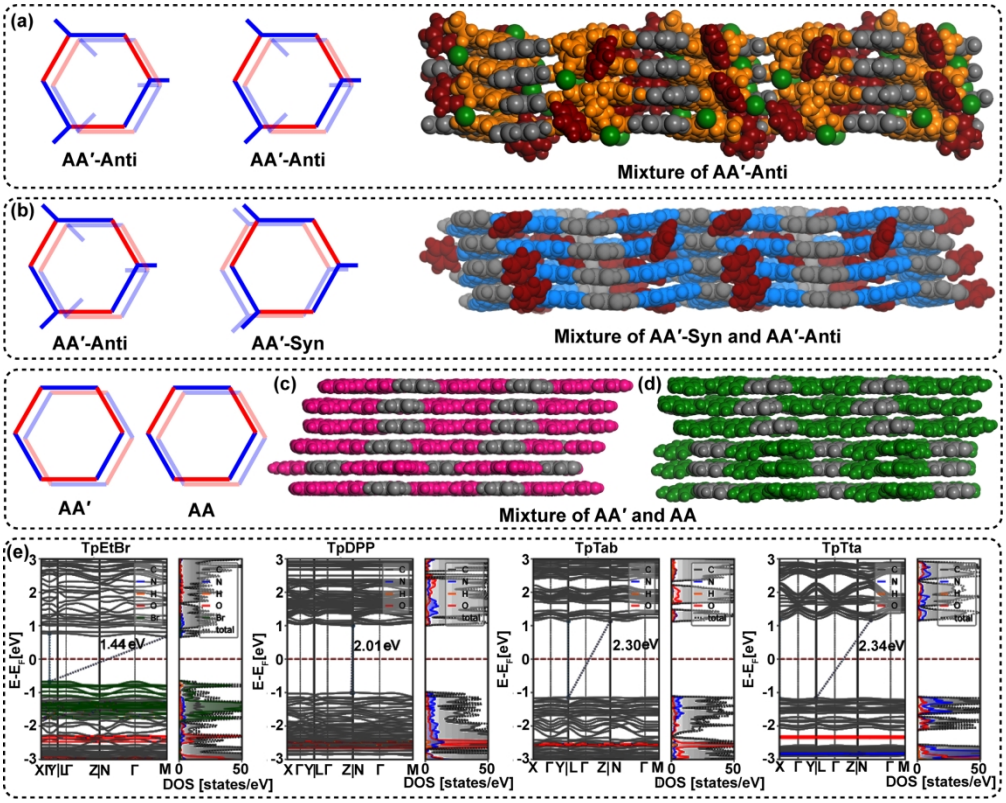

Figure 3

239x190mm (300 x 300 DPI)

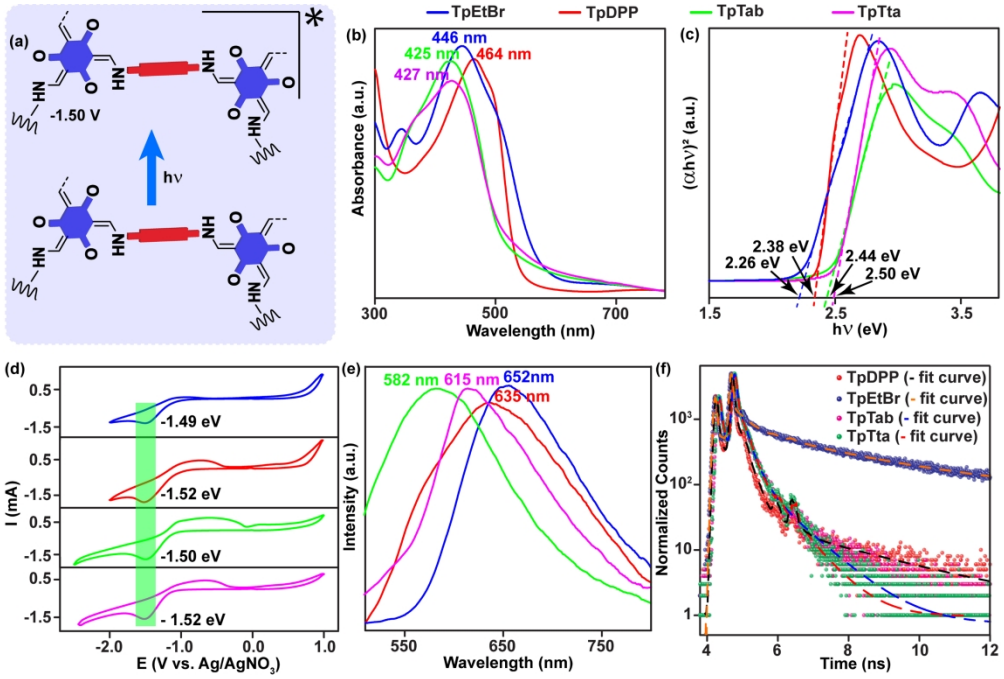

Figure 4

277x185mm (300 x 300 DPI)

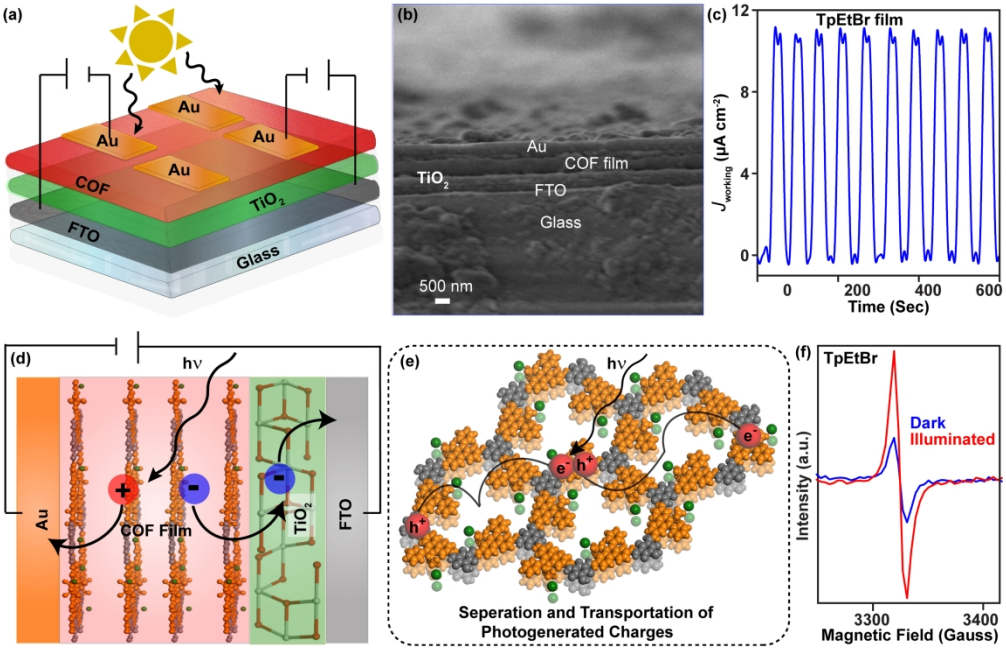

Figure 5

294x189mm (300 x 300 DPI)

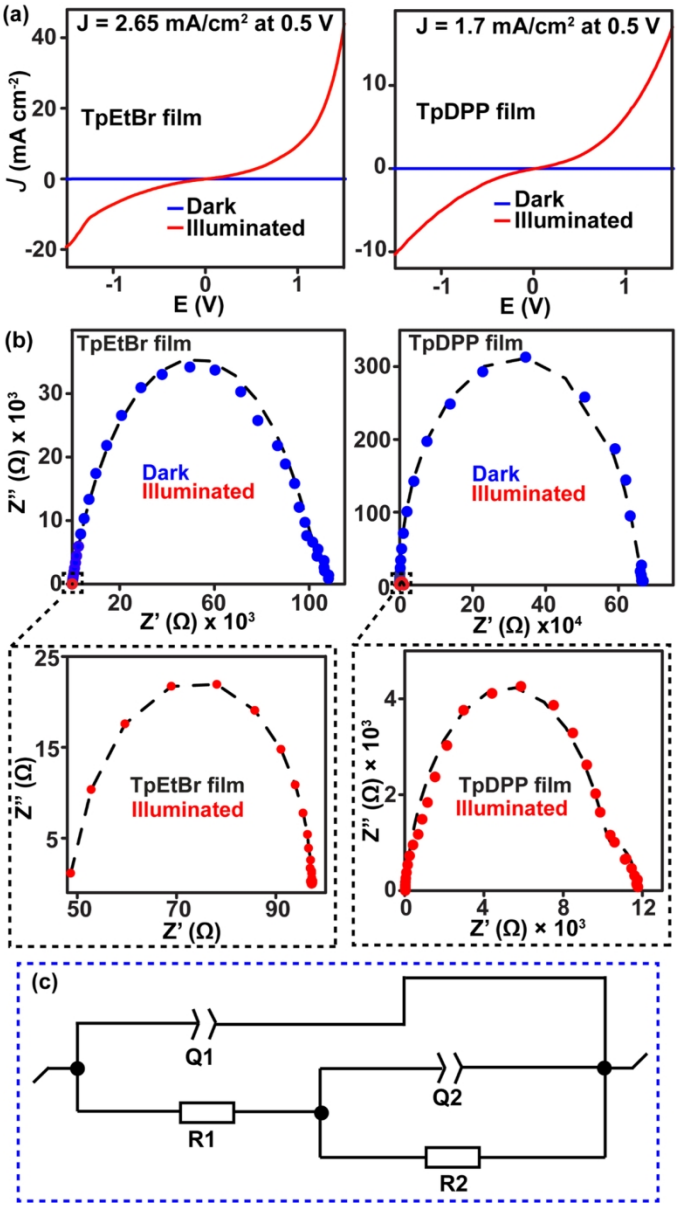

Figure 6

107x190mm (300 x 300 DPI)

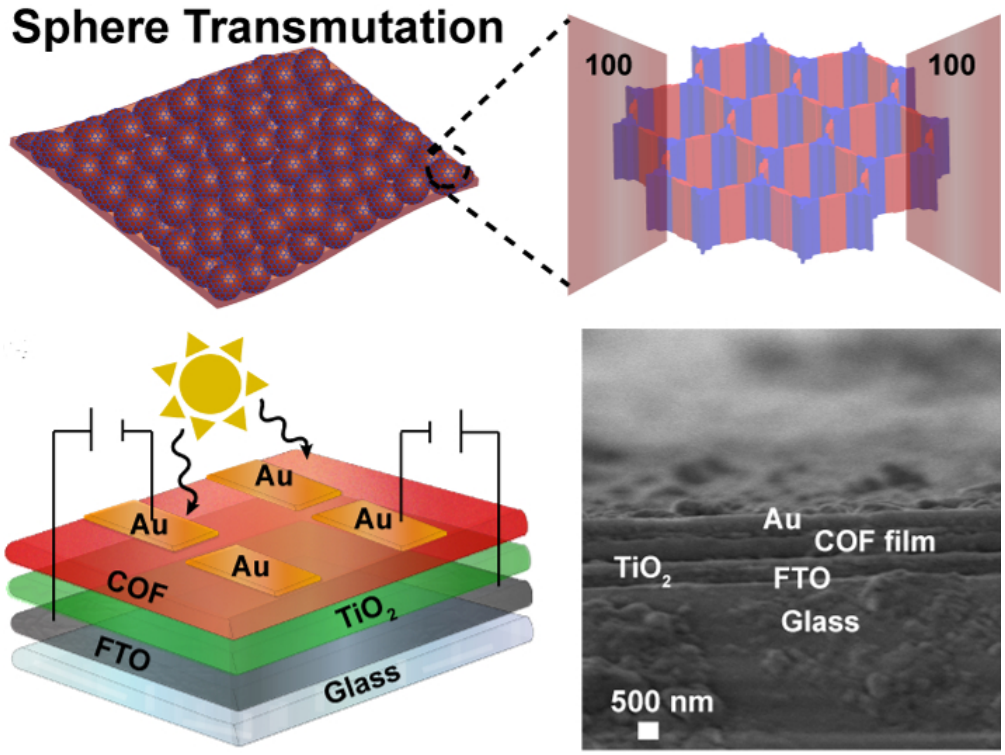

Figure TOC

60x45mm (300 x 300 DPI)